DIGITIZED PRECISION MEASUREMENTS OF THE MOVEMENTS OF SEA URCHIN SPERM FLAGELLA

ROBERT RIKMENSPOEL AND CHERYL A. ISLES
Department of Biological Sciences, State University of New York, Albany, New York 12222

ABSTRACT High speed cinemicrographs were made of sea urchin sperm at temperatures varying from 22 to 6°C. Apparatus, combining a television camera and a video digitizer, was constructed to scan individual flagellar images and to digitize the flagellar waveforms. With appropriate smoothing and averaging procedures, the rough data were condensed by a microcomputer into the coordinates of 20 points along a flagellum, spaced 2 μm apart. The curvature of the flagellum at these points was also computed. The coordinates of the flagellar positions were obtained to an accuracy of approximately ± 0.1 μm, flagellar curvature to an accuracy of approximately ± 50 cm^{-1}. At all temperatures the amplitude of the flagella was found to vary with time in a purely sinusoidal fashion to within $\pm 2\%$. The local curvature of the flagella had basically a purely sinusoidal time course to within ± 50 cm^{-1}, but a varying amount of asymmetry was present in the distal and the proximal ends of the flagella. This asymmetry in the curvature was related to the radius of the circular path of the sperm. The flagellar waveforms can probably be summarized in simple algebraic functions.

INTRODUCTION

It is now generally accepted that a sliding filament mechanism, with the dynein molecules forming cross-bridges between adjacent tubulin microtubules, is responsible for the force generation in flagella and cilia (Summers and Gibbons, 1971). The analogy of the mechanism in flagella and cilia to that in striated muscle has encouraged the development of mathematical models for the force production in axonemes, which can be seen as descendents of the work of A. F. Huxley (1957). Some of the models have used purely analytical procedures (Rikmenspoel, 1971, 1978*b*; Lubliner and Blum, 1972; Brokaw and Rintala, 1974). On the other hand, the simple structure of the axoneme, with nine logitudinal fibers between which cross-bridges can form, makes the axoneme a very suitable object for the formulation of precise molecular models. Such models in which the attachment and detachment of every dynein cross-bridge is followed as a function of time have indeed been developed successfully to obtain waveforms that simulate those in live flagella and cilia (Brokaw, 1972; Rikmenspoel and Rudd, 1973; Rikmenspoel, 1976, 1982; Hines and Blum, 1978, 1979).

To judge how well a model describes actual flagellar or ciliary motion, it is necessary to compare computed results with observations on living specimens. Quantitative data on the waveforms of flagella and on the time course of the events within a cycle of motion are at present scarce. Recent model work on sea urchin sperm flagella (Rikmenspoel, 1982) has shown that the time course of the internal, active moments produced by the formation of dynein cross-bridges, is displayed directly in the time course of the local curvature of the flagella. The curvature and its variation with time are thus sensitive indicators of the force producing processes in a flagellum. The results of these calculations indicate that meaningful comparisons of computed results with observed motion data require that the curvature of the flagella be measured to an accuracy of ± 50 cm^{-1}. This represents ~2 to 3% of the maximal curvatures observed in live sea urchin sperm flagella. Conclusions about the time course of the internal active moments in flagella could be made when the time course of the motion within a cycle is measured to an accuracy of approximately ± 0.1 μm.

Measurements of the curvature of sea urchin sperm flagella and of its variation as a function of time have been made by Rikmenspoel (1978*a*) and by Hiramoto and Baba (1978). The time course of the curvature within a cycle of motion was found by these authors to be roughly sinusoidal. The accuracy of the reported data fell short of that stated above as required for meaningful comparisons with model calculations, however.

In this laboratory a program has been started to obtain precision data on the motion of sea urchin sperm flagella. Apparatus was built to make high quality dark-field cinemicrographs of the sea urchin sperm. An instrument was developed that can scan the photographic sperm images, and digitize and store the flagellar coordinates and curvatures in a computer memory for further analysis. This paper describes the instrumentation and the results obtained with live sea urchin sperm in the temperature range of 6–22°C. Special attention was given to the time course of the events within a cycle of motion.

EXPERIMENTAL METHODS AND APPARATUS

Preparations

Sea urchins of the species *Arbacia* were obtained from the Marine Biological Laboratory (Woods Hole, MA). Sperm shedding was induced by injection of 1–2 ml of 0.5 M KCl into the body cavity of sea urchins. The spermatozoa were suspended in filtered sea water at pH = 7.8.

A few drops of sperm suspension were placed on a microscope slide and covered with a 180-μm thick coverslip. The thickness of the fluid layer of the sperm suspension was ~20 μm. The slide was placed on the stage of a Zeiss universal microscope (Carl Zeiss, Inc., Thornwood, NY). Viewing and filming was done with dark-field illumination using a Zeiss ultracondensor (NA = 1.4) and a Zeiss oil immersion 40× objective (NA = 0.85) (Carl Zeiss, Inc.). Films were made within 5–6 min after slide preparation.

Temperature Control

A polyethelene bag, secured both at the base and above the objective nose piece, enclosed the lower part of the microscope. The focus and mechanical stage knobs protruded through openings in the bag. Cold air, with a temperature varying from 4 to −10°C, depending on the desired temperature of the sperm preparation, was blown through the bag thus cooling the lower part of the microscope. The temperature was measured away from the direct airstream with a mercury thermometer and with a thermistor taped to the objective. These two temperatures agreed with each other to within 2°C. Temperatures of the experimental preparations mentioned below in the Results section were those measured with the thermistor.

Cinemicrography

The light source for dark-field illumination was a 1,000 W xenon arc lamp (type 982C-1; Conrad-Hanovia, Hanovia Lamp Division, Newark, NJ). The lamp was operated in a flashing mode by a steering circuit analogous to that described previously (Eykhout and Rikmenspoel, 1960). For each flash, a condensor of 100 μF at 200 V was discharged, giving an electrical input of 1.6 J/flash. Almost square light pulses of slightly <100-μs duration were obtained.

In between light flashes and when preparing for filming, the xenon arc lamp must be kept ionized by a direct current of 10–15 A. The resulting constant light output was not sufficient to register the sperm flagella on the film; it was used to advantage for viewing and focusing the preparations. Ultraviolet and infrared radiation from the lamp was eliminated with 3-mm GG420 and 6-mm KG3 glass filters (Schott and Gen., Mainz, Federal Republic of Germany).

Precise measurement of flagellar positions requires the presence of good fiducial markings. For this purpose a grid of fine glass wires of 20μm thickness was cemented in the field diaphragm of the projection eyepiece of the microscope. The glass wires were illuminated from the side, through a window machined in the projection eyepiece, by a 300 W quartz halogen projection lamp (type ELH; General Electric Co., Cleveland, OH). To obtain sharp imaging of the glass wire grid onto the photographic emulsion, it was necessary to screen off all but the center 2 mm of the top lens of the eyepiece.

Cinemicrographs at 400 or 200 frames/s were made on 16mm Kodak #2514 emulsion (Eastman Kodak Co., Rochester, NY). This film is extremely fine grained but consequently rather insensitive. Fig. 1 illustrates the quality of the photographic imaging obtained. The final magnification (using a 5 × projection ocular) on the 16mm emulsion was ~60 ×.

Digitizing Equipment

Of sperm selected for detailed analysis, sequences of up to 70 consecutive 16-mm frames were rephotographed and enlarged ten times on 35-mm Kodak #2514 emulsion (Eastman Kodak Co.). On these rephotographed images, the sperm and the reference lines appear bright on a dark background. Apparatus was constructed to automate the analysis of the rephotographed images.

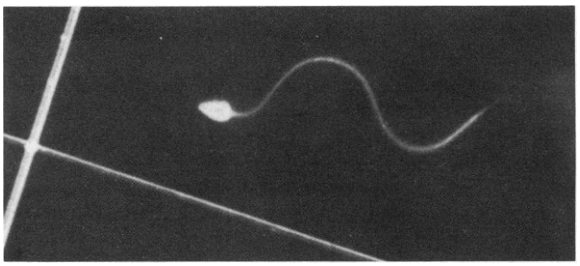

FIGURE 1 Positive enlargement of a part of a 16-mm film frame showing an *Arbacia* sperm is pictured. The reference lines, which act as fiducial markings for defining the absolute position of the sperm, were photographed with the preparation as described in the text.

In principle the apparatus consists of a television camera that scans the projected image of a rephotographed sperm. The output of the television camera is fed into the digitizer and a microcomputer that computes the coordinates and the curvature of a number of points along the flagellum. Details of the instrument and its operations are given below.

The sperm images were projected onto a tracing table at a final magnification of 2,510 × by a 35-mm film strip projector (model SM1000; Singer Education Systems Inc., Rochester, NY). Highly transparent and fine grained Mylar drafting film (Keuffel and Esser Co., Morristown, NJ) served as the projection screen. A Fresnel lens with a focal length of 50 cm and having 2 lines/mm (Edmund Scientific Co., Barrington, NJ) was mounted 2 cm below the projection screen. This lens concentrated the light from the projector onto the objective of the television camera (model SV650; Dage-MTI Inc., Michigan City, IN) situated 1 m above the projected image.

Fig. 2 shows a diagram of the image seen at the Mylar projection screen. The reference lines shown define the position of the sperm in the preparation. These reference lines could not be used directly as a set of coordinate axes because they were not perfectly straight and perpendicular to each other. Instead, the reference lines were traced out, and an external X,Y axes system was drawn on the Mylar screen, as shown in Fig. 2. When a new photograph was projected, the Mylar screen was shifted so as to align the reference lines.

A slit arrangement, shown diagrammatically, in Fig. 3, was placed over the projected image of the spermatozoon. The slit, driven by a synchronous motor, scanned the sperm image from the head towards the tip as shown in Fig. 3. The overhead television camera thus observed a section of the sperm flagellum, which during a scan moved distally.

The whole slit assembly was mounted on a Paragon drafting machine (Keuffel and Esser Co.). This made it possible to displace the slit arrangement parallel to itself and to change the direction in which the scanning took place, as indicated in Fig. 2. The angle ϕ (see Fig. 2) of the scanning direction relative to the X,Y axes could be read directly from the vernier on the drafting machine.

The television camera was mounted such that it could be rotated on its optical axis. In actual use the lines of the television raster were always parallel to the slit. The magnification of the objective of the television camera was chosen so that the image of a sea urchin sperm covered about ¾ of the height of the television monitor screen. The video system thus operated in its own coordinate system, with a different orientation and magnification from that at the optically projected image. To avoid confusion the optical coordinate system, which was fixed to the sperm preparation, will be written in capitals (X, Y), and the video coordinate system in lower case (x, y).

The television camera probes the image along the raster lines from left to right and from top to bottom. The video digitizer (model 622; Colorado

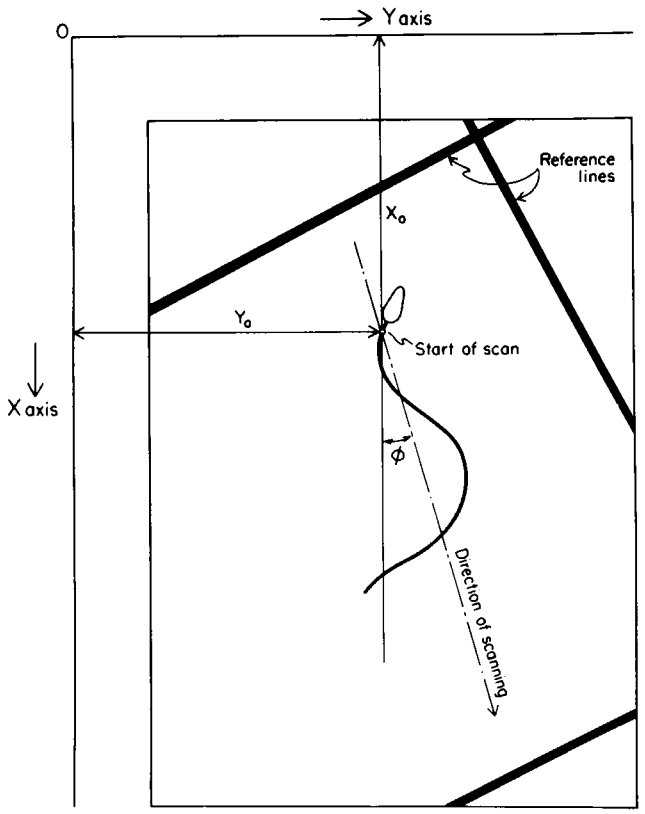

FIGURE 2 A diagram of the image at the Mylar projection screen is shown. The reference lines correspond to those visible in Fig. 1. The X and Y axes are the coordinate system fixed to the sperm preparation.

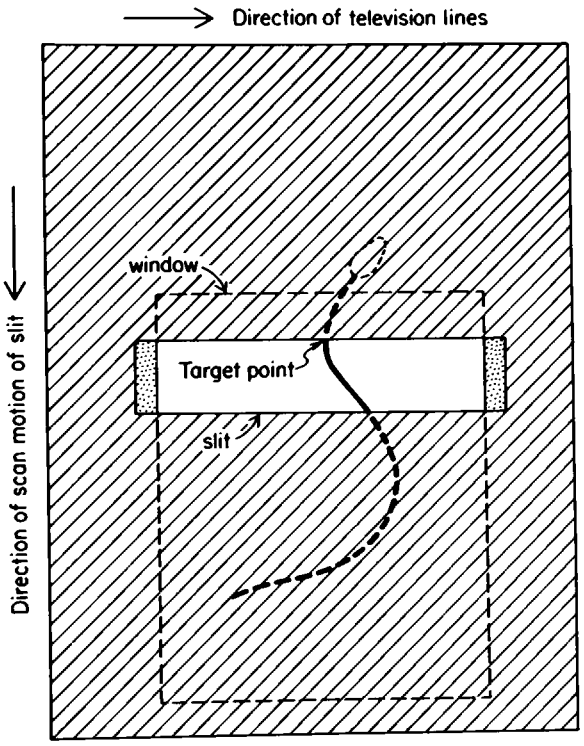

FIGURE 3 A diagram of the slit arrangement for scanning the sperm image is shown. The target point is the point of which the x and y coordinates are determined by the digitizer, as explained in the text. The slit width of 15 mm serves to insure that a sufficiently large segment of the flagellum is exposed for the automatic gain control of the television camera to function properly.

Video, Boulder, CO) determined 60 times per second the y coordinate of the first point encountered at which the light intensity is above a preset discrimination threshold. During the scanning of the photograph by the slit, this target point, indicated in Fig. 3, moved uniformly down the x direction. The x coordinate of the target point was thus given by the time elapsed since the start of the scan. The y position of the target point, as determined by the digitizer was fed into a microcomputer (model 5-15D; Altos Computer Systems, San Jose, CA). During the scan of a flagellum, the microcomputer received an array of ~700 points. The location of a member in the array thus gave an x coordinate and the value of the array member a y coordinate. Since the image of a sperm flagellum, as shown in Fig. 1, has a finite width, these coordinates represented the position of points on the edge of the flagellum as seen by the television camera. In the x direction the points were spaced ~0.05 μm apart.

After the initial adjustments of the projected image were made, a point at 2 μm from the proximal junction of the flagellum was marked off by hand as the start of the scan of the flagellum. The coordinates X_0 and Y_0 of the starting point (see Fig. 2) and the angle ϕ of the scanning direction were entered by hand into the microcomputer. The scanning of the flagellum was then started and repeated one to four times dependent on the quality of the photographic image.

The microcomputer was programmed to average the y arrays obtained in the repeated scans of a photograph. The data were then smoothed and reduced to the absolute X and Y coordinates of a set of points, spaced at a distance s = 2 μm, on the center line of the flagellar image. For each of these points the local curvature of the flagellum was computed. For every photograph the absolute coordinates and the curvature of 20 points at 2-μm intervals along the flagellum were thus obtained. The details of the somewhat complicated computing procedures are given in the Appendix. After the analysis of a series of photographs was completed the data were transferred to a Univac 1180 computer (Sperry Corp., Philadelphia, PA). All further data analysis was done on that machine.

Data Analysis

The average path of a sperm was computed as a circle fitted through a superposition of the points of the middle section of the flagellum ($10 < s < 30$ μm) on all photographs analyzed for that sperm. The amplitude at each of the 20 points along the flagellum was then calculated as the deviation of that point from the average path. This is completely analogous to the data reduction done previously by hand (Rikmenspoel, 1978*a*).

To study the time course of the flagellar motion, the amplitude or the curvature at one fixed location on the flagellum must be followed as a function of time. When these data are plotted *vs.* time, one obtains a time series for the amplitude on the curvature at a particular location on the flagellum. Examples of such time series are given below in Figs. 5, 7, and 15. We wish to detect systematic patterns in these time series, since model calculations (Rikmenspoel, 1982) have indicated that the kinetics of the attachment and detachment of the dynein cross-bridges are displayed in patterns in the time series. For a pattern to be systematic it must repeat itself from period to period. The time series studied should therefore be as long as possible. The series obtained in the present experiments covered from four to six periods of the flagellar motion. The limits were set in practice by the length of the time interval the sperm could be observed without physical or optical interference.

In the present experiments, the period of the flagellar motion was found to vary by up to 10% over the length of the time series. Since the period was not perfectly constant, it was not possible to fit a sine curve to the time

series and then study the residuals, as was done previously (Rikmenspoel, 1978*a*). Instead, Fourier analysis has been performed on the time series.

In Fourier analysis, the Fourier transform $g(\nu)$ for the time series is calculated

$$g(\nu) = b\int_0^{t_1} f(t)\, e^{-2\pi\nu i}\, dt, \qquad (1)$$

where $f(t)$ represents the time series, the time interval $0 - t_1$, is the length of the time series, and b is a normalization constant. The integral in Eq. 1 was computed with the trapezoidal rule and a time interval equal to the time between photographs.

When the absolute value $|g(\nu)|$ of $g(\nu)$ of Eq. 1 is plotted *vs.* the frequency, ν, the Fourier spectrum of the time series is obtained. The flagellar frequency shows in the Fourier spectrum as a high peak. Systematic deviations of the time series from being purely sinusoidal are displayed in the Fourier spectra by secondary, harmonic peaks with a frequency that is an integer multiple of the main frequency.

The theory of Fourier analysis of very long time series has been treated by Wiener (1963). The capabilities and limitations for time series of ~50 points covering four to six periods appear not to have been published. We have therefore investigated the application of Fourier analysis to time series with a known content of harmonic components. As a general conclusion we have found that from time series such as those in the present experiments, up to the seventh harmonic component is readily detectable. The peak height represented the content of a harmonic component to approximately ±20% standard deviation (SD).

In the measurements reported below, the time series sometimes contained <10 points per period. This occurred mainly for sperm with a flagellar frequency much above 40 Hz. Useful spectra were obtained for these sperm, but the high frequency end of the spectra had to be disregarded.

RESULTS

Arbacia sperm preparations were filmed at temperatures of 22, 16, 12, and 6°C. The average flagellar frequency of the sperm in each sample was determined. Spermatozoa that were free of hindrance and near to, but not crossing, the image of reference lines were selected for detailed analysis. Eight sperm were analyzed at 16 and 22°C, seven sperm at 6°C, and four sperm at 22°C. The number of photographs analyzed for each sperm varied from 35 to 67 with an average of just under 50. For two of the sperm a complete set of reference lines was not within the field of view of the 35-mm camera. For those cells, absolute coordinates were thus not available and only data on the curvature of the flagella were obtained. The radius of the average path of these sperm was determined by hand as previously described (Rikmenspoel, 1978*a*).

Performance of the Digitizing Equipment

For routine operation of the video-digitizing apparatus, good uniformity of the photographic contrast along the flagellar image was required. Minor imperfections in the photographs, such as scratches or dust spots were occasionally corrected by pencil shading applied to the area. To determine the accuracy of the measurements of the flagellar coordinates and curvatures, one cannot use artificially constructed images of curves and line segments. Errors introduced during the process of filming actual sperm preparations are eliminated by the use of artificial curves, and a false impression of accuracy would be obtained. Instead, we have derived figures for the accuracy from the scattering of the data obtained from live sperm.

Fig. 4 shows an overlay of the coordinate points measured by the digitizing equipment onto an enlargement of the flagellum for two flagellar positions. Since no reliable way was available to transfer the coordinate system of the Mylar projection screen (see Fig. 2) directly onto the enlarged photographs, Fig. 4 was constructed as follows. The coordinate points put out by the computer were plotted on transparent graph paper to a scale of 1 cm = 2 μm. The graph paper was aligned over a photograph at the corresponding magnification to have maximal coincidence of the plotted points with the center of the photographic image of the flagellum. The plotted points and the coordinate system were then transferred to the photograph by pinpricks. When the original of Fig. 4 was viewed under low-power optical magnification, the distance of the points from the center of the flagellar images could be directly read. The SD of the points from the flagellar center was SD = 0.07 μm. When repeated analyses were made of one single photograph, the SD of the position of the points along the flagellum was ±0.07 μm.

Above, the accuracy of measurements within single photographs was determined. When a series of photographs is analyzed, additional errors are introduced by deformations of the film material, variations in photo-

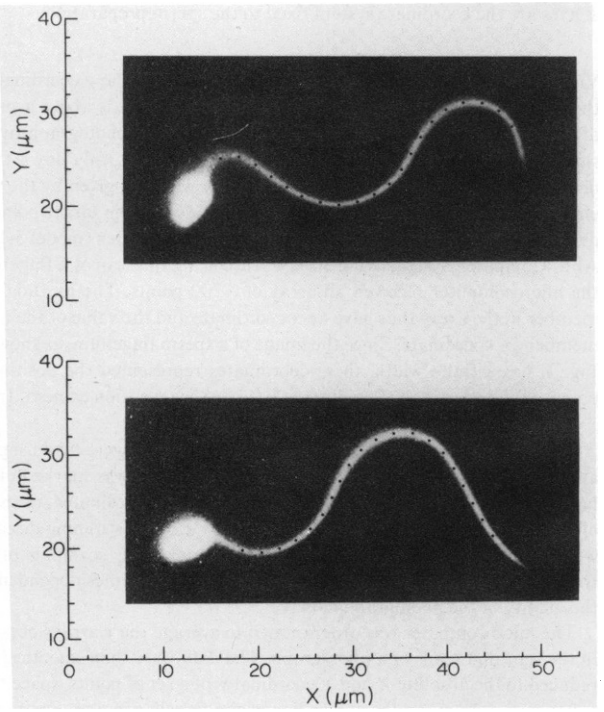

FIGURE 4 Two flagellar positions of sperm No. 11 at a 10-ms interval is shown. The dots on the flagella represent the coordinate output of the digitizing equipment. The figure was constructed as described in the text. The photographic prints were made such as to maximize the width of the flagellar images to avoid fusing the plotted points with the background.

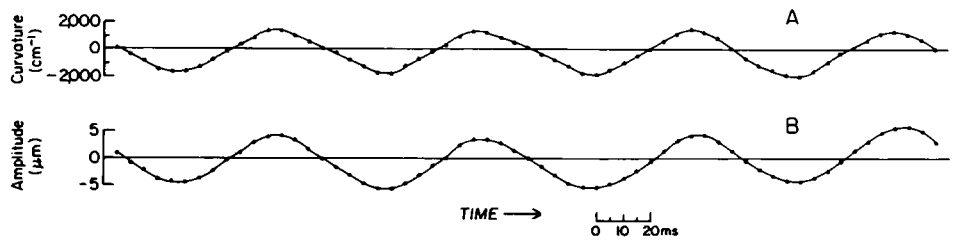

FIGURE 5 A time series for the curvature (A) and the amplitude (B) for sperm No. 19 at a distance $s = 20$ μm from the head. The deviations of the points from the smooth line drawn by eye gives an impression of the accuracy of the measuring procedure.

graphic quality, and the uncertainties of defining the starting point of the scan and positioning the slit assembly. The smoothness of the time series in those cases where many points are present per cycle of flagellar motion gives an impression of the accuracy of the total measuring procedure. Fig. 5 B shows the time series for the amplitude of a sperm with ~15 photos per cycle of motion. The SD of the plotted points from a smooth line drawn by eye through the points (when plotted on an expanded scale) was SD = 0.14 μm. Through one single period in the time series in Fig. 5 B a sine curve could be fitted with a SD equal to 0.08 μm. The above results together indicate that the flagellar coordinates can be measured with the digitizing equipment to an accuracy of close to ±0.1 μm.

Fig. 6 shows the curvature as a function of the distance along the head, measured twice. When multiple measurements were made of the curvature along the flagellum, the SD of the values was ±45 cm^{-1}. No alternative way to measure the local curvature of the flagellum was available, and therefore no independent check of the absolute accuracy of the curvature measurements could be made. The maximum curvature shown in Fig. 6 is very close, however, to the average curvature of almost circular flagellar segments reported previously (Rikmenspoel, 1978*a*).

Fig. 5 A displays the time series for the curvature of a sperm with nearly 15 photographs per cycle of motion. When a smooth line was drawn by eye through the points in Fig. 5 A (plotted on an expanded vertical scale) the SD of the points from this line was SD = 65 cm^{-1}. We have concluded that the curvature of the flagella could be measured with an accuracy of nearly ±50 cm^{-1}.

Near the distal tip of the flagellum, the performance of the apparatus was sometimes degraded if the tip of flagellum had moved out of focus or was oriented in a direction nearly parallel to the television raster line. Fig. 7 A shows a time series for the amplitude at $s = 38$ μm from the head. It can be seen that one point, indicated by the arrow, is far from the smooth line drawn through the points. The Fourier spectrum of the time series in Fig. 7 A is shown in Fig. 7 B. The background in the high frequency end of the spectrum is close to 10% of the height of the main peak. When the one outlying point in the time series was corrected to a value corresponding to the smooth line in Fig. 7 A, the spectrum shown in Fig. 7 C was obtained. The spectrum of the corrected time series has a background of ~2%.

Fig. 7 illustrates that when time series are investigated, not a single measurement can be seriously in error. Only spectra with a background of <5% of the height of the main peak have been included in the section on the time course of events below. This means in practice that all spectra from time series containing even a single error of the kind shown in Fig. 7 A were excluded. Note that in all results reported below, no corrections were applied.

Wave Properties as a Function of Temperature

Fig. 8 shows an Arrhenius plot of the average flagellar frequency of the sperm samples at the various temperatures. The straight line through the points in the range 10–22°C shows a $Q_{10} = 2.2$. This is close to the value of Q_{10}

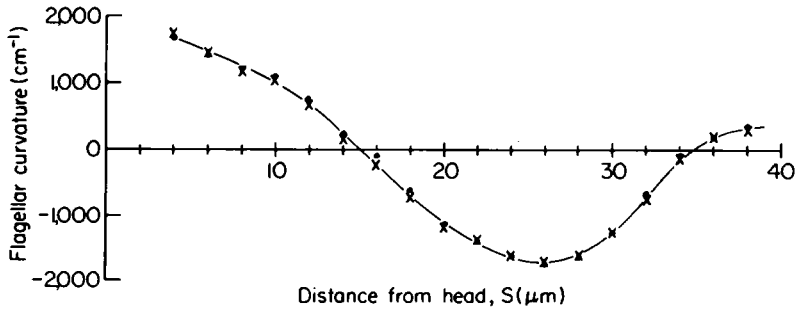

FIGURE 6 Curvature of sperm No. 11 (*bottom* position in Fig. 4) on two consecutive measurements, represented by × and ●, respectively, as a function of the distance from the head, s is shown.

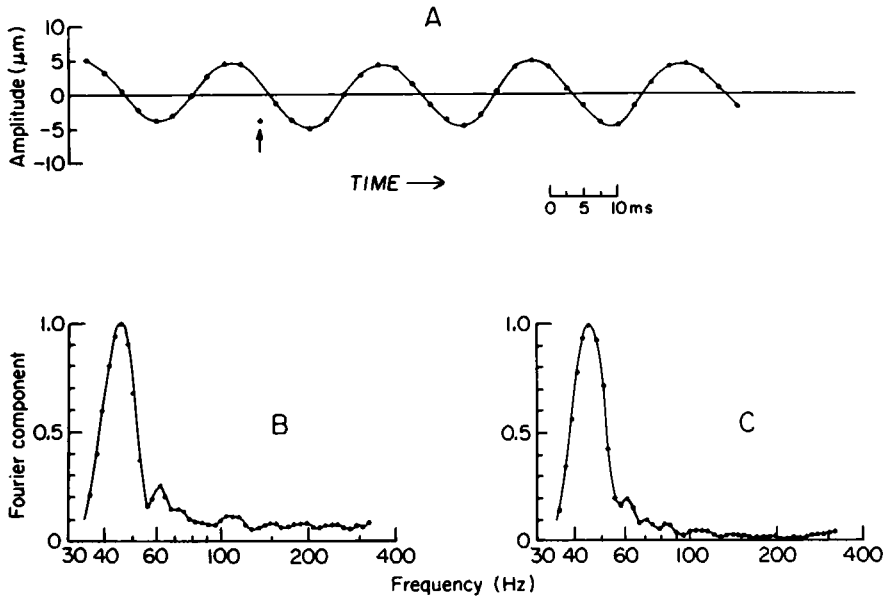

FIGURE 7 (*A*) Time series for the amplitude at $s = 38$ μm of sperm No. 6 is shown. The point indicated by the arrow is far from the smooth line drawn by eye through the points. (*B*) Fourier spectrum of the time series in Fig. 8 *A* is shown. The background of the high frequency end of the spectrum is close to 10% of the height of the main peak. (*C*) Fourier spectrum of the time series in Fig. 8 *A* with the point indicated by the arrow corrected to lie on the drawn line is shown. The background of the spectrum is ~2%.

= 2.1 reported previously for bull spermatozoa (Rikmenspoel, 1983) and for the flagella of *Crithidia oncopelti* (Coakley and Holwill, 1973). A sudden drop of the flagellar frequency for temperatures below 10°C has been observed in the other species also.

The flagellar frequencies found for *Arbacia* in the present experiments appear slightly higher than those reported in other sea urchin species at corresponding temperatures (Gibbons and Gibbons, 1980; Brokaw, 1966; Gray, 1955). The possible causes for this discrepancy are mentioned in the Discussion.

The wavelength, measured along the flagellum, was obtained for the sperm analyzed from the phase shift of the time series as previously explained (Rikmenspoel, 1978*a*, 1983). Fig. 9 shows the wavelengths of the sperm at the various experimental temperatures, plotted against the flagellar frequency. The wavelength shows a very weak dependency on the flagellar frequency over the range 7.5–82 Hz. This agrees with the observations of Brokaw and Josslin (1973) that the wavelength of demembranated sea urchin sperm is only slightly increased when the flagellar frequency is lowered by a reduction in the external ATP concentration.

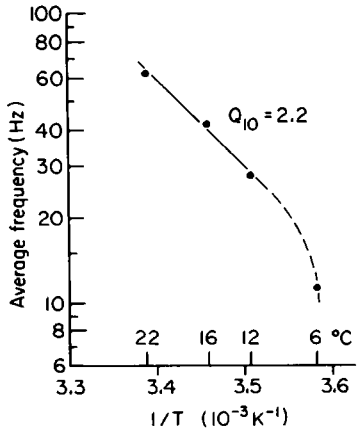

FIGURE 8 Arrhenius plot of the average frequency of *Arbacia* sperm is shown. The straight line drawn by eye indicates a $Q_{10} = 2.2$ for the flagellar frequency in the range 10–22°C.

The amplitude of the flagellar wave motion was maximal in the middle section of the flagellum, around $s = 20$ μm, and decreased towards both ends, in accordance with earlier observations (Rikmenspoel, 1978*a*; Hiramoto and Baba, 1978). Fig. 10 shows the maximum amplitude of the sperm in the present experiments, plotted against the flagellar frequency. It can be seen that the wave amplitude increases very slightly towards the low frequencies, which represent sperm at the lowest temperature. The broken line in Fig. 10 is the amplitude as a function of the flagellar frequency expected when the internal active moment is constant over the frequency range. The line was derived from model calculations published previously (Rikmenspoel, 1982). The data in Fig. 10 suggest that at 6°C the internal active moment of the sperm is decreased compared with that at higher temperatures, but that at the higher temperatures (12–22°C) it is rather constant.

The curvatures observed varied considerably along the flagellum. The maximum curvature at each location was taken as one half of the peak-to-peak variation in the time series of that location. At each of the four experimental temperatures, the variation between the sperm of the

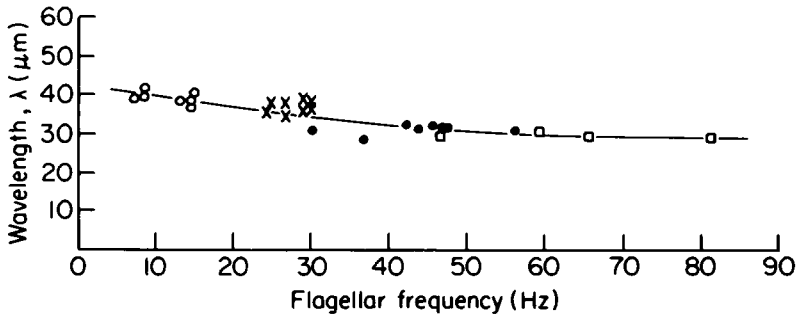

FIGURE 9 Wavelength, λ, measured along the flagellum, for *Arbacia* sperm as a function of frequency is shown. The different symbols each indicate one sperm at various temperatures: □, 22°C; ●, 16°C; x, 12°C; ○, 6°C. The line was drawn by eye.

maximal curvature at a given location along the flagellum was rather small. In Fig. 11 *A* is plotted the average, over the sperm in the sample, of the maximal curvature at 16 and 12°C as a function of the location on the flagellum. It can be seen in Fig. 11 *A* that the curvatures increase sharply towards the proximal junction. In the more distal parts of the flagella, the curvatures are rather constant even though a small systematic trend is present. There is no indication in Fig. 11 *A* that the curvatures vanish at the distal tip of the flagella, in agreement with earlier observations (Rikmenspoel, 1978*a*; Hiramoto and Baba, 1978).

The data in Fig. 11 *A* suggest that at 12°C the curvature are slightly lower than at 16°C. In Fig. 11 *B* the curvatures, averaged over the sperm at each temperature, at 4, 8, and 20 μm from the head are plotted as a function of temperature. It can be seen in Fig. 11 *B* that in general the curvatures decrease weakly with the temperature. The effect is small, however, compared with the variation of the curvature with the location on the flagellum.

The data in Figs. 9–11 suggest that the effect of lowering the temperature of the sperm was only to slow down the flagellar motion. No sharp variation of wave properties with the temperature was evident. It appears that the various sperm can be treated as one sample showing only a weak dependence of wave properties on the flagellar frequency in the range of 7.5–82 Hz.

Time Course of Amplitude and Curvature

The time course of the events within a flagellar cycle is given by the time series for the amplitude and the curvature and their Fourier spectra. After omitting those spectra that showed a background of 5% or more of the height of the main peak, ~400 spectra were obtained for each the amplitude and the curvature. The sperm were treated as one continuous sample over the flagellar frequency range of 7.5–82 Hz. Most of the spectra were not plotted, but features were read directly from the digital printout. All spectra discussed below were normalized to a main peak height equal to 1, with the height of a spectral feature given in percentage of the height of the main peak.

In the spectra, second, third, fourth, and fifth harmonic components were observed. Spectral features were identi-

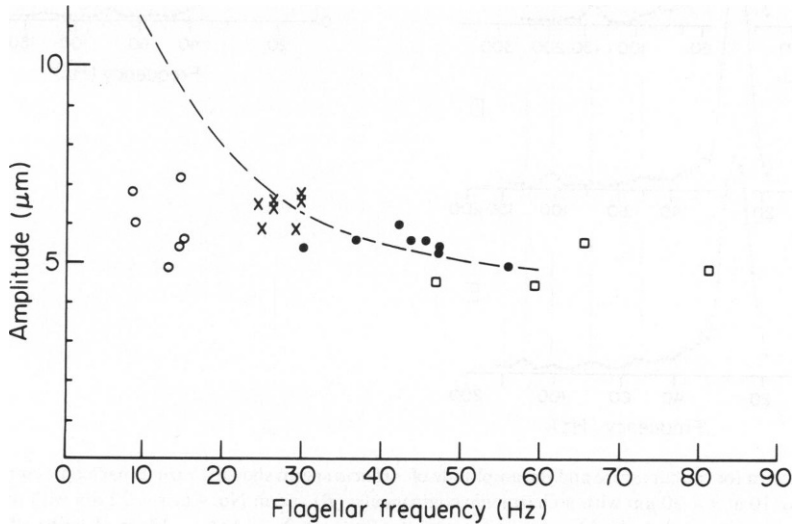

FIGURE 10 Maximum amplitude of the flagellar waves in *Arbacia* sperm as a function of the flagellar frequency at various temperatures: □, 22°C; ●, 16°C; x, 12°C; ○, 6°C is shown. The dotted line represents the amplitude as a function of flagellar frequency expected for a constant internal active moment, as derived from model calculations (Rikmenspoel, 1982).

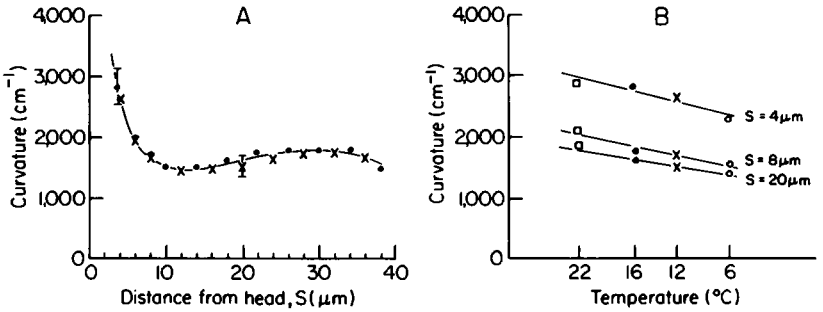

FIGURE 11 (*A*) Curvature, averaged over the sperm at each of two temperatures of the preparation, as a function of the distance from the head, *s* is shown. (*B*) Average curvature at three different locations along the flagellum as a function of temperature is shown. The vertical bars indicate typical standard deviations over the sperm at each temperature. The lines in Figs. 11 *A* and *B* were drawn by eye; □, 22°C; ●, 16°C; x, 12°C; ○, 6°C.

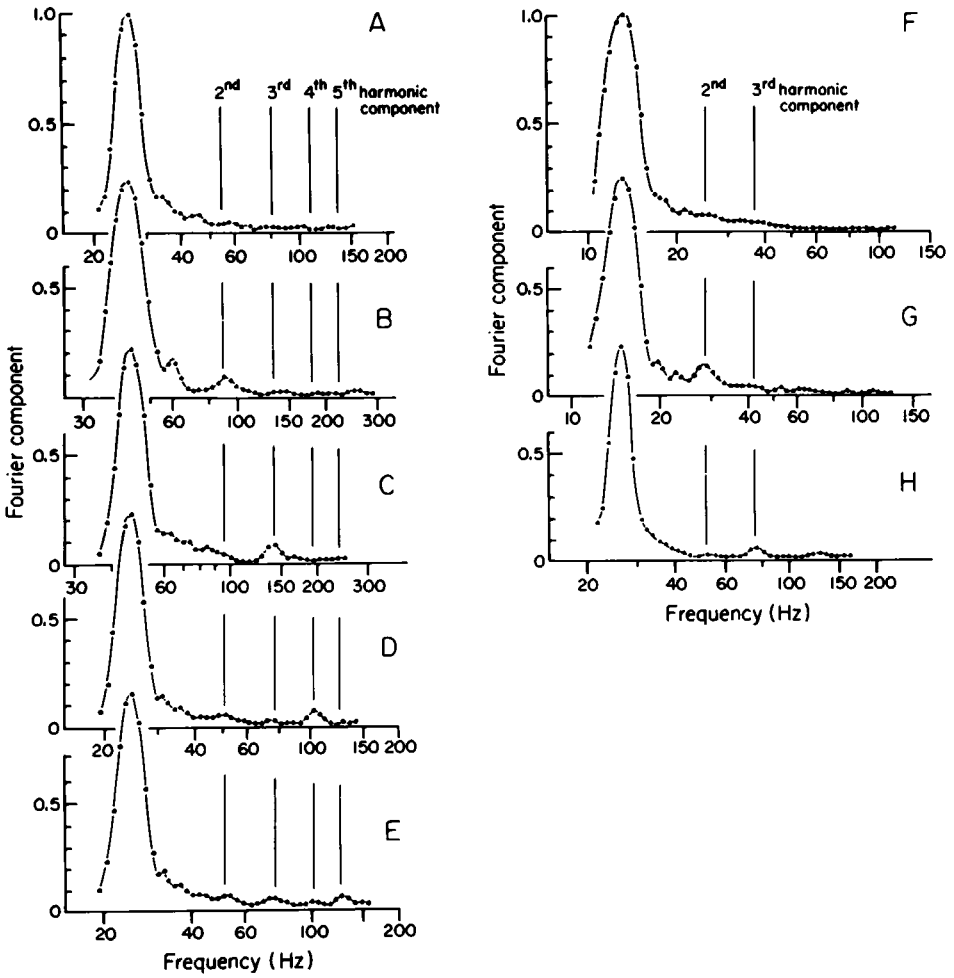

FIGURE 12 Fourier spectra for the curvature and the amplitude of *Arbacia* sperm showing various harmonic components are shown. For the curvature (*A*) sperm No. 10 at $s = 30$ μm with no harmonic components; (*B*) sperm No. 4 at $s = 22$ μm with only a second harmonic; (*C*) sperm No. 1 at $s = 22$ μm showing only a third harmonic component; (*D*) sperm No. 14 at $s = 12$ μm showing a fourth harmonic; (*E*) sperm No. 14 at $s = 14$ μm with a small fifth harmonic component. An indication of some content of second, third, and fourth harmonic is visible in this spectrum. For the amplitude (*F*) sperm No. 19 at $s = 6$ μm with no harmonic components; (*G*) sperm No. 23 at $s = 28$ μm with a second harmonic component; (*H*) sperm No. 13 at $s = 14$ μm showing a third harmonic component.

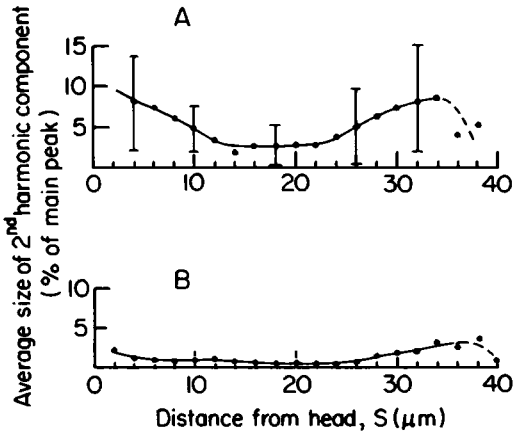

FIGURE 13 Second harmonic component averaged over all sperm as a function of location on the flagellum is shown: (*A*) curvature; (*B*) amplitude. The vertical bars indicate typical SD.

fied as harmonic components if their frequency was within 2 to 3% of an integer multiple of the flagellar frequency, if the height of the peak was at least 2% of the height of the main peak, and if the peak stood out clearly above the background of the spectrum. Components with a peak height of <2% were rounded off to 0.

Fig. 12 shows examples of Fourier spectra without any harmonic content, and of spectra in which a second, third, fourth, or fifth harmonic component of ~6–10% was present. The spectrum of Fig. 12 *E* shows, besides the fifth harmonic component, some indication of small second, third and fourth components. Spectra for the amplitude showing only a clear fourth or fifth harmonic component were not encountered. The various harmonic components will be discussed separately below.

Second Harmonic Components

Second harmonic components were found in many of the Fourier spectra for the curvature. The largest second harmonic component had a peak height of 24%. The distribution of the peak heights of these harmonics was strongly concentrated towards the smallest values. Roughly two-thirds of the spectra contained 4% or less of second harmonic, only 1 out of 20 spectra showed 15% or more of second harmonic. In the spectra for the amplitude the second harmonic components occurred less often, and they were of smaller magnitude. Approximately three-fourths of the spectra contained a second harmonic component of 2% or less. These results suggest that the absence, or the presence of only a very small, second harmonic component in the Fourier spectra for both the curvature and the amplitude should be considered the norm.

Fig. 13 *A* and *B* show the distribution along the flagellum of the second harmonic component, averaged over all spectra, for the curvature and the amplitude, respectively. The second harmonic components in the curvature spectra occur mostly at the proximal and distal ends of the flagella as indicated in Fig. 13 *A*. Therefore three sections of the flagella were considered separately: s = 4–10 μm, s = 14–20 μm, s = 30–32 μm.

The average amount of second harmonic component over the flagellar section s = 4–10 μm sperm is strongly correlated with the inverse of the radius of the average path, R, as shown in Fig. 14 *A*. It can be seen in Fig. 14 *A* that the sperm at the various temperatures do not appear to favor either a smaller or a larger radius of the average path.

A second harmonic component in the Fourier spectrum is related to a deformation of the time series from a purely sinusoidal shape. The precise form of this deformation is given by the phase of the second harmonic relative to the phase of the main component. The phase of the Fourier components, given by the phase factor of $g(\nu)$ in Eq. 1 above, changes sharply near any spectral feature. In the analysis performed for the present experiments, the phase at the peak of the harmonic components could not be determined very accurately.

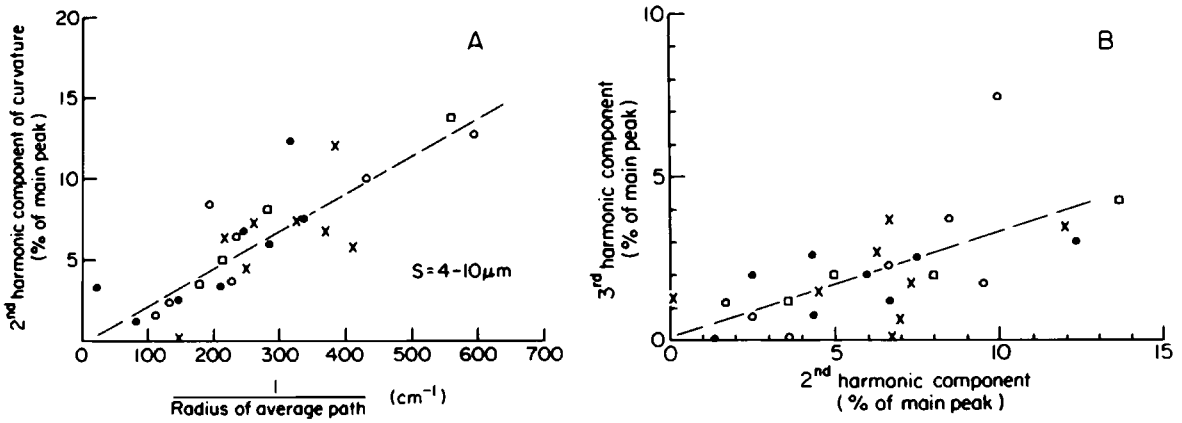

FIGURE 14 (*A*) Relation between the second harmonic component in the curvature spectrum and the inverse of the radius of the average path of the sperm is shown. (*B*) Relation of the average size of the second and third harmonic components in the curvature spectrum for the proximal part of the flagellum (s = 4–10 μm) is shown. □, 22°C; ●, 16°C; x, 12°C; ○, 6°C.

The actual deformation could, however, be seen directly in the time series for those cases where a large second harmonic component was present. Fig. 15 *A* shows a time series for the curvature at $s = 4$ μm, near to the head. The Fourier spectrum of this time series in Fig. 15 *C* shows a large second harmonic component of close to 20%. It can be seen in Fig. 15 *A* that the time series is quite noisy. This was often found at locations near the head. The pattern in the time series is also not completely constant. Only a minor part of these irregularities is due to instrumental measuring error, and most of it should be considered inherent to the sperm motion.

Fig. 15 A illustrates that the deformation resulting in the second harmonic component, is an asymmetry of the time series that is visible as a flattening of the tops of the curves. The asymmetry illustrated in Fig. 15 *A* can be expected to be caused by an asymmetry in the motion of the sperm. This agrees well with the results in Fig. 14, which show a correlation between the size of the second harmonic component, and the radius, *R*, of the average path of the sperm.

In the flagellar section $s = 30$–32 μm, a correlation between *R* and the average second harmonic component in the curvature spectra might be present. The large scattering of the data precluded a secure interpretation of the data, however. In the spectra for the amplitude, the second harmonic component was distributed rather evenly over the flagellum as can be seen in Fig. 13 *B*. The average size of the second harmonic was between 1 and 2%, except in the extreme distal part of the flagellum where it reached 3%.

The size of a second harmonic component in the Fourier spectra of the amplitude and the curvature were not correlated. This is illustrated in Fig. 15 where the Fourier spectrum for the amplitude at $s = 4$ μm shows a second harmonic component of ~2% (Fig. 15 D). The time series for the amplitude in Fig. 15 *B* is not perceptibly deformed from a sine curve. The time series for the curvature at the same location (Fig. 15 *A*) shows the large asymmetry discussed above, resulting in the second harmonic in the Fourier spectrum of close to 20% (Fig. 15 *C*).

Third Harmonic Components

In the Fourier spectra for both the curvature and the amplitude, small third harmonic components were found. A third harmonic content of 2% or less was observed in two-thirds of the spectra for the curvature and three-fourths of those for the amplitude. The distribution along the flagellum of the third harmonic component was rather uniform, as shown in Fig. 16 *A* and *B* for the curvature and amplitude, respectively. The average size of the third harmonic component was ~2% for the curvature and 1% for the amplitude.

In the proximal section of the flagella, the amount of third harmonic component in the curvature spectra was correlated with the amount of second harmonic compo-

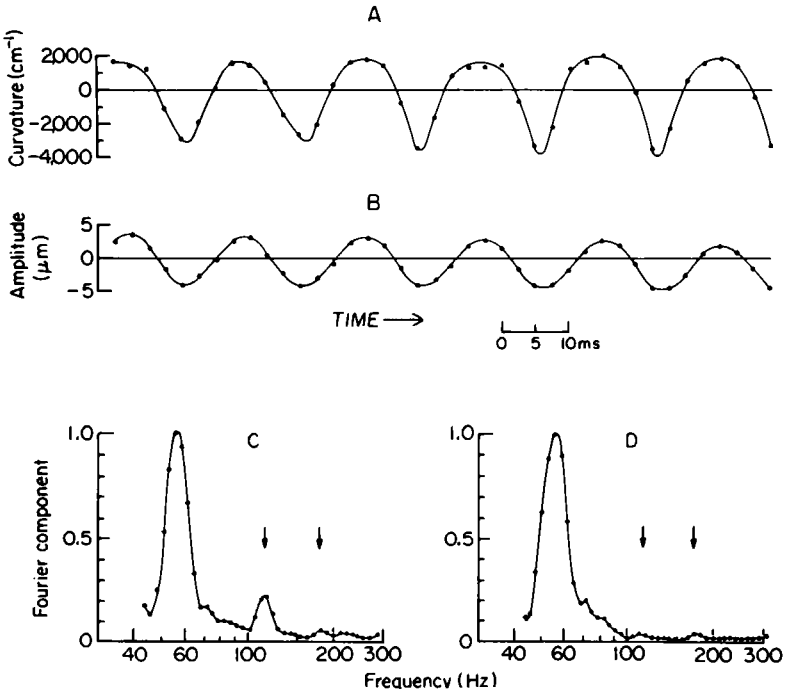

FIGURE 15 Time series for sperm No. 8 at $s = 4$ μm for the curvature (*A*) and the amplitude (*B*) are shown. (*C*) Fourier spectrum of the time series in Fig. 15 *A* for the curvature is shown. The arrows indicate the position of the large second and the small third harmonic components. (*D*) Fourier spectrum of the time series for the amplitude in Fig. 15 *B* is shown. The arrows indicate the small second and third harmonic components.

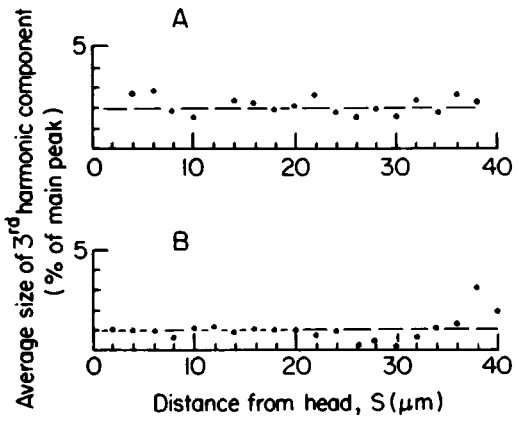

FIGURE 16 Third harmonic component, averaged over all sperm as a function of location on the flagellum is shown; (*A*) curvature; (*B*) amplitude.

nent, as shown in Fig. 14 *B* above. It can be seen that the third harmonic component is roughly one-third of the size of the second. At the more distal locations on the flagella ($s > 10$ μm), no correlation between the size of the second and the third harmonic was found. Any existing correlations could easily have been overwhelmed by the scatter of the data, however.

Fourth and Higher Harmonic Components

In 45 of the Fourier spectra for the curvature (equal to 12% of the total number of spectra) a fourth harmonic component was observed. The largest component was 6%. Averaged over all spectra the content of fourth harmonic component was 0.4%. In 14 of the spectra for the amplitude (equal to 3.5% of the total number) a fourth harmonic component, with a maximum size of 4%, was present. The average content over all spectra was 0.1%.

For three sperm, at four or five locations each, the Fourier spectra for the curvature showed a fifth harmonic component of 2 to 4%. Fifth harmonic components were not present in any spectra for the amplitude. No sixth or seventh harmonic components were identified with certainty in the spectra for either the curvature or the amplitude.

Waveforms

The waveforms of the sperm analyzed, represented by the coordinates of the points at 2 μm spacing along the flagella, were stored in the computer memory. These sets of waveforms are in practice only useful if they could be summarized in simple algebraic expressions. The results of the analysis of the time course of the flagellar motion above suggest the manner in which this might be accomplished.

The main harmonic components of consequence found were second harmonics in the spectra for the curvature. As discussed above, these second harmonics were related directly to the radius of the (circular) average path of the sperm and indicated an asymmetry. It would appear logical to conclude that the waveforms represent a shape that has become asymmetrical by bending. This is basically a geometrical argument with no assumptions made concerning the mechanism in the sperm causing the effect.

Fig. 17 *A* shows a sine curve, which is obviously a symmetrical shape. If this curve is plotted along a bend axis, the shape in Fig. 17 *B* is obtained. Fig. 18 *A* shows five flagellar waveforms, at 10-ms intervals, of a typical sperm. In Fig. 18 *B* each of the flagellar waveforms is represented by a single segment of the bent sine curve shown in Fig. 17 *B*. The similarities between the waveforms of the live sperm and the simulated shapes are apparent.

Close inspection of Figs. 18 *A* and *B* shows that the real and the simulated waveforms do, however, differ from each other in important details. The sharp curvature near the head in the live sperm is absent in the simulated ones. The curvature in the midsection of the live flagella is varying more smoothly than that in the bent sine curves.

It appears that the symmetrical curve, which by bending yields the flagellar shape, should be a slightly deformed sine curve. Theoretical treatments of the expected waveshapes of passive and active sea urchin sperm flagella (Machin, 1958; Rikmenspoel, 1978*b*) have led to a representation of the waveshapes by a superposition of deformed sine curves. The functions used by Machin (1958) and Rikmenspoel (1978*b*) are therefore the logical candidates for algebraic expressions for the flagellar waveforms, with the appropriate bending as illustrated in Fig. 21. Because

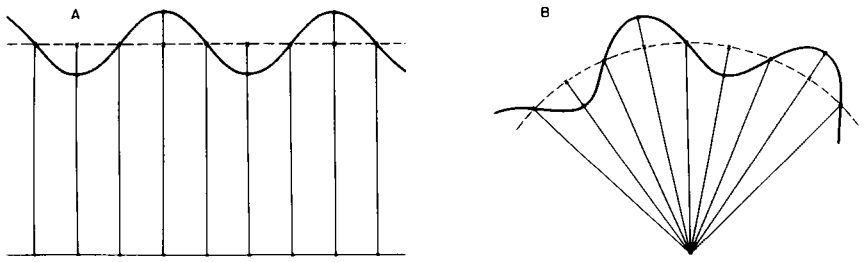

FIGURE 17 (*A*) Sine curve plotted on a straight axis is shown. (*B*) The process of plotting the curve of Fig. 17 *A* on a bend axis is illustrated.

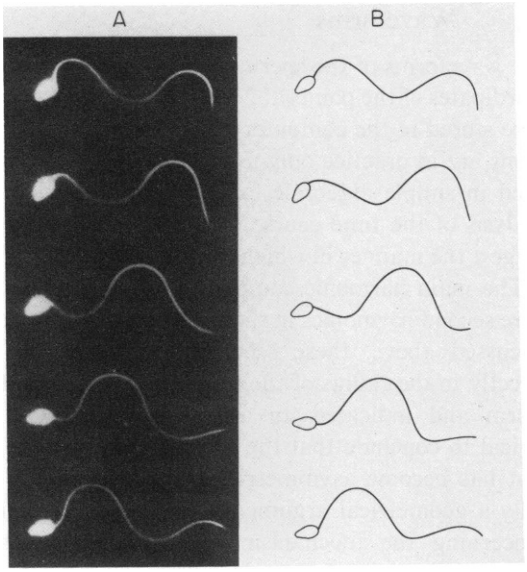

FIGURE 18 (*A*) Five flagellar positions at 10-ms interval of sperm No. 15 are shown. (*B*) Simulation of the flagellar waveforms by segments of the curve in Fig. 17 *B* is shown. Each of the simulated flagellar shapes consists of a single segment of the bend sine curve.

this represents a rather mathematical subject, it will be treated separately in a theoretical journal.

DISCUSSION

The occasional fourth and fifth harmonic components in the Fourier spectra of the curvature are probably due to irregularities in the motion of the sperm flagella that do not have any significance. The data show a clear trend in that the harmonic components become smaller and less frequent at higher orders. It seems, therefore, extremely unlikely that higher order harmonic components beyond the limit of the seventh observable in the present experiments, are present in the time course of the curvature or the amplitude. The only meaningful features in the time course of the flagellar cycle appear to be the second and third harmonic components.

In general, a second harmonic component indicates the presence of an asymmetry in the time series from which the Fourier spectrum was derived. This can be seen as follows. If the angular frequency of the main period of the time series is written as ω, with $\omega = 2\pi \times$ flagellar frequency, the second harmonic Fourier component $F(2)$ can be written as $F(2) = a \cos(2\omega t)$. This can be rewritten as

$$F(2) = 2a\cos^2(\omega t) - a. \qquad (2)$$

Eq. 2 shows that the deformation caused by the second harmonic component $F(2)$ repeats with the same period as the main component. Since the square of a cosine is inherently positive, the effect of $F(2)$ on the positive and the negative part of the main component will be different, leading to an asymmetry.

The time series shown in Fig. 15 *A* illustrates that for the case of the spermatozoa considered in this paper, the asymmetry consisted of a flattening of the tops on one side of the time series. To simulate this, the Fourier spectrum was determined for a purely sinusoidal time series, flatly truncated on one side as shown in Fig. 19 *B*. The Fourier spectrum of this time series is shown in Fig. 19 *A*. A large second harmonic component can be seen in the spectrum, while a third harmonic component of approximately one-third the size of the second is present. By varying the amount of the truncation of the tops of the time series it was found that the size of the second harmonic component in the spectra was approximately proportional to the truncation. The ratio of the second and third component remained roughly constant at 3:1 in the range of truncation of 0 (a full sine curve) to 0.6 (shown as the time series in Fig. 19 *B*).

A flattening of the tops on one side of the time series for the curvature thus explains the occurrence of the second and the smaller accompanying third harmonic component in the Fourier spectra. Since the time course of curvature of the flagella has been predicted from model calculations to follow the time course of the internal moments (Rikmenspoel, 1978*b*), the most probable cause of this flattening of the tops is a saturation of the active moment on one side of the flagellum. That more active moment is developed on one side of the flagellum compared with the other, leads then logically to a curved path.

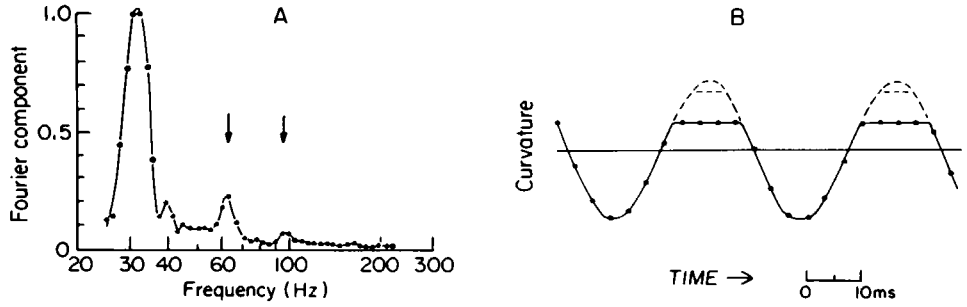

FIGURE 19 Fourier spectrum (*A*) of a time series in the shape of a truncated sinc curve (*B*) is shown. The large second harmonic component and the small third one in the spectrum are reminiscent of those in Fig. 15 *C*. The dotted lines at the tops in Fig. 19 *B* show a truncation of 15%, as discussed in the text.

For most sperm in the present experiments, the asymmetry is much smaller than that illustrated in Figs. 15 and 19. These examples were selected to make the effects readily visible. Fig. 14 shows, however, that 11 of the 27 sperm in our present sample had a second harmonic component of 5% or less in the Fourier spectrum of the curvature for the proximal section of the flagella. This corresponds to a truncation in the time series of 15% or less as indicated in Fig. 19 *B*. It appears that for model calculations the time course of the curvature in the proximal section should be considered to be purely sinusoidal. A small but varying perturbation, probably due to a saturation of the active moment at one side of the flagellum, should be introduced to account for the observed asymmetries.

The asymmetry in the curvature of the sperm flagella near the head has been noticed before. It has led to a description of the motion towards one side as the principal bend and of that to the other side as the "reverse bend" (Goldstein, 1975; Gibbons and Gibbons, 1980). The present results as discussed above indicate that probably two distinct phenomena are not present, but that instead one general bending phenomenon is slightly disturbed on one side.

The simplest explanation for the observed asymmetry seems that one or more of the peripheral fibers on one side of the axoneme have a limited ability to produce forces. In sea urchin sperm extracted with Triton X-100 in the presence of a small amount of Ca^{2+}, the asymmetry of the flagellar waves is increased (Okuno and Brokaw, 1981). A determination of the site and the mode of action of Ca^{2+} in this increase of the asymmetry would probably clarify the cause of the asymmetries in general (Gibbons and Gibbons, 1984).

In the middle part of the flagellum ($10 < s < 30\ \mu m$) the curvature and the active moment should be considered to have a purely sinusoidal time course. The features observed in the Fourier spectra for that section amount to a few percent. These are probably due to transient irregularities in the motion.

Both the second and the third harmonic components in the spectra for the amplitude showed a strong concentration towards the smallest values. These harmonic components also appear to be randomly distributed along the flagella (Figs. 13 *B* and 16 *B*). Most probably they represent irregularities in the motion and not meaningful systematic effects. The time course of the amplitude at all locations on the flagella should therefore be considered to be purely sinusoidal to the limits of detection in the present experiments of ~2%. This 2% variation means that the time course of the amplitude (which is maximally $\simeq 5\ \mu m$ for sea urchin sperm) is sinusoidal to within $\pm 0.1\ \mu m$.

Recent model calculations (Rikmenspoel, 1982) have indicated that in sea urchin sperm, the flagella can act as a mechanical filter. The result of such a filtering would be that the temporal details of the internal active moments in the flagella are not displayed in the transverse motion. The present experimental findings appear to confirm the model prediction that deviations from a sinusoidal time variation are seen in the curvature, but not in the amplitude of the flagella.

As was stated above, it is likely that the asymmetry in the time course of the curvature and the general bend shape of the sea urchin sperm flagellum have a common cause. A quantitative explanation of these effects can only be expected from a proper formulation of an asymmetric perturbation in an otherwise symmetric model. To be ultimately convincing, however, the precise variation of the curvature asymmetry along the flagellar length, the absence of an asymmetry in the amplitude, and the curved shape of the sperm should all follow from a single perturbation.

The main conclusion arrived at above was that the mechanochemical mechanisms in the flagella should be formulated to give rise to purely sinusoidal oscillations. In biochemical oscillatory systems (Higgins et al., 1973) and in the mechanochemical system of insect flight muscle (Pringle, 1967), such sinusoidal oscillations have been reported. From rest, full flagellar motility can develop within one single period of motion in sea urchin sperm (Gibbons and Gibbons, 1980; Rikmenspoel, 1978*a*). These fast transitions were not observed in the systems of Higgins or Pringle, and they should be considered a special property of sea urchin sperm flagella.

No attempts have been made to derive patterns for the sliding of the microtubules in a flagellum. Previous reports of the conversion of flagellar waveforms into data on the sliding of microtubules (Yano and Miki-Noumura, 1980; Goldstein, 1979) have been based on the assumption that the microtubules are not extensible. However, using reasonable estimates for the elastic modulus of the tubulin fibers and for the forces produced by the dynein cross-bridges, a stretching of the tubulin fibers that is comparable to the amount of assumed sliding can be expected during flagellar motion (Rikmenspoel, 1982). A certain caution should probably be exercised when deriving quantitative sliding data from observations of the flagellar waveforms.

In the section entitled Waveforms, the expectation was held that the flagellar waveforms can be reduced to simple algebraic expressions. The formulation in purely analytical form of the processes in flagella would become more meaningful in that event. It would not imply that numerical models incorporating precise molecular details have become superfluous. The comparison of the results of such calculations with the experimental data would be greatly facilitated, however.

The wavelength of the *Arbacia* sperm was found to vary weakly with the flagellar frequency and with the temperature of the preparation. At the lower temperatures, the active forces produced inside the sperm flagella appear to be much reduced, as indicated in Fig. 10. This suggests that the flagellar wavelength is not determined by the

contractile processes in the flagella. On the basis of other observations, this conclusion has been expressed before (Okuno and Brokaw, 1979; Rikmenspoel, 1978*a*). The wavelength in a passive sea urchin sperm flagellum, neglecting all internal active force production, has been calculated previously (Rikmenspoel, 1966). The predicted wavelengths are shown by the band in Fig. 20, which is reproduced from Rikmenspoel (1966). The wavelength, $\lambda(x)$, in Fig. 20 was calculated in small amplitude approximation. This corresponds to the wavelength projected onto the average path of the sperm. For the sperm in our sample, $\lambda(x)$ was computed and the values were inserted in Fig. 20. Apparently the wavelength variation with the flagellar frequency is adequately described by the simple elastic theory. These results reinforce the belief expressed previously (Okuno and Brokaw, 1979; Rikmenspoel, 1978*a*) that the wavelength in sea urchin sperm flagella is determined mainly by elastic properties of the flagella and that it is not much influenced by the internal force producing processes.

The data in Fig. 10 suggest that the internal active moments in sea urchin sperm do not vary much with the temperature in the range 12–22°C, but that they are much decreased at lower temperatures. This differs from the behavior of bull sperm flagella (Rikmenspoel, 1983), where the internal active moments decreased monotonously and strongly in the range 4–37°C. Possibly, this represents a case of evolutionary adaptation. In normal physiological conditions, bull spermatozoa are exposed only to a constant female body temperature of 37°C. Sea urchin spermatozoa, on the other hand, are shed in sea water that has a natural and considerable temperature variation.

The average value for the flagellar frequency of the sea urchin sperm in the present paper shown in Fig. 8, was ~40 Hz at 16°C. This is higher than the values reported previously by other authors (Gray, 1955; Brokaw, 1966; Gibbons and Gibbons, 1980), which range from 30–35 Hz at comparable temperatures. The temperature of the preparation cannot be measured directly while employing an immersion objective and condensor. Spermatozoa in the field of view of the microscope are exposed to the illuminating light. Even though a very effective filtering of the infrared portion of the illuminating light was employed in the present experiments, it cannot be excluded that the temperature of the illuminated portion of the preparations was ~2°C higher than the temperatures stated. This would explain the apparent discrepancy between our present data and those reported previously. None of the other results or conclusions above would be affected, however.

The digitizing equipment has performed satisfactorily for the live sperm considered here. In most experimental conditions, artificialities are introduced that lead to a reduction of flagellar activity (for a review, compare Gibbons, 1981). In these conditions the apparatus would be equally useful. Occasionally invertebrate sperm display waveforms characterized by a strongly increased curvature (Brokaw, 1966; Cosson et al., 1983). These sperm then have flagellar sections that are nearly perpendicular to the overall axis of the sperm. In the television image of photographs of these sperm, flagellar sections would be parallel or near parallel to the raster lines, making successful digitizing impossible. A special adaptation of the apparatus would be necessary for these sperm. Alternatively, the sperm could be divided into sections that are scanned separately.

APPENDIX

The reduction of the rough data in the microcomputer proceeded in eight successive steps.

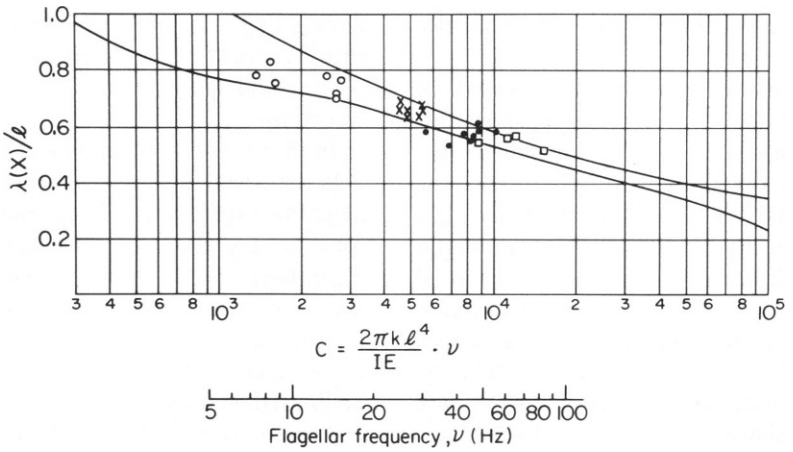

FIGURE 20 Wavelength of sea urchin sperm flagella calculated under neglect of all active internal moments is shown. The running variable is the flagellar frequency, ν, multiplied by a constant $2\pi k\ell^4/IE$ representing the ratio of viscous and elastic forces on the flagellum; k, viscous drag coefficient; ℓ, flagellar length; and IE, stiffness of the flagellum. The band depicts the range of the predicted wavelength due to the possible variations in boundary conditions. (Redrawn with permission from *Biophys. J.*, 1966, 6:955). The points represent the measured values for the sperm in the present experiments: □, 22°C; ●, 16°C; x, 12°C; ○, 6°C.

(*a*) The values for the y arrays obtained in the repeated scans were averaged and via the precalibrated magnification of the television system and the known traveling speed of the slit, converted into microns. This resulted in two arrays giving the x and y coordinates in microns of ~700 points along the flagellum.

(*b*) Occasionally the digitizer produced a wrong number in the y array, due to internal noise, due to dust particles in the light path, or due to a photographic irregularity. Starting at the second member of the y array, for each member, y_n, of the array the difference from the previous member, y_{n-1}, was therefore calculated. If this difference was ≥ 1 μm, the member y_n was taken as being in error. When the next following member, y_{n+1}, was not found to be in error ($|y_{n+1} - y_{n-1}| > 1$ μm), y_n was corrected to $y_n = (y_{n+1} + y_{n-1})/2$. In the event y_{n+1} was also in error ($|y_{n+1} - y_{n-1}| \leq 1$ μm), the value of y_n was corrected to $y_n = y_{n-1}$. The y array was thus scanned and corrected for errors. The total number of corrections made was displayed on the computer monitor. In actual usage, most photographs were scanned without needing a single error correction. Approximately six error corrections for one photograph were judged to be the maximum permissible.

(*c*) After the error corrections the y array showed a noise equivalent to 0.2 to 0.3 μm. The array was smoothed by replacing each member y_n by $y'_n = (y_{n-1} + 2y_n + y_{n+1})/4$ (Johnston et al., 1979). For the first member, y, this procedure is, of course, not possible. Instead we have used $y'_1 = 2y'_2 - y'_3$. Eight successive smoothing passes over the array were made. The finally obtained smoothed y array showed a noise of <0.01 μm. The above smoothing algorithm is very effective in reducing the noise in the array without altering the flagellar shape it represents. The procedure can be interpreted as an averaging of the y coordinates of the flagellum over a length of several tenths of microns with the weight of the adjacent array members distributed according to the binomial formula.

(*d*) The smoothed y array represents the coordinates of points along the left-side edge of the flagellum. To obtain the position of the center of the flagellar image, the y coordinates must be shifted by one-half of the width of the flagellar image. This width can vary along the flagellum. When, however, the objective of the television camera is adjusted very slightly out of focus, the flagellar image as seen by the television camera near the top of the slit is rounded off (the width of the flagellar image away from the top of the slit is unaffected, however). The target point detected by the digitizer is then on the rounded portion of the flagellar image, as illustrated in Fig. 21. In practice, the target point is displaced from the flagellar center line by an amount rather independent of (but smaller than) the width of the image.

The angle θ of the flagellar center line with the x axis affects the correction for the width of the flagellar image to be made, as can be seen in Fig. 21. θ was computed for the neighborhood of each array member. The array member was corrected by $W/\cos\theta$, with an empirically determined value of $W = 0.15$ μm maintained throughout all results reported.

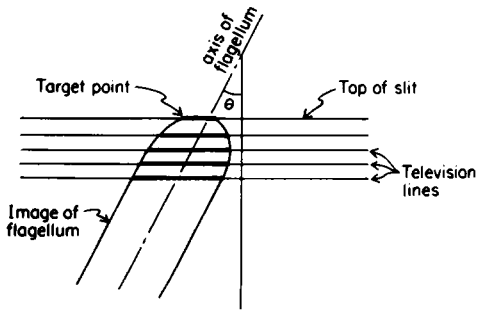

FIGURE 21 (*A*) An enlarged diagram of the television image of the section of the sperm flagellum visible to the television camera near the top of the slit is shown. The enhanced portions of the television scan lines indicate the area where the light intensity is above the discriminator level of the digitizer.

(*e*) After the correction for the flagellar width the y and the x arrays represent the coordinates of points on the center axis of the flagellum. The first array member represents the coordinates $x(1)$ and $y(1)$ of a point at a distance $s = 2$ μm from the proximal flagellar junction. Those array members were selected which were at an equal distance of 2 μm, measured along the flagellum, from each other. The final representation of the coordinates of the flagellum was thus a string of 20 coordinate sets $x(N)$, $y(N)$, ($N = 1, \ldots, 20$) representing points at a distance from the flagellar junction $s(N) = N \times 2$ μm.

(*f*) For a determination of the curvature at the Nth flagellar point the array members representing a flagellar segment of 2-μm long on either side were fitted to a Taylor series

$$y(n) = f(a) + \frac{f'(a)}{1!}[x(n) - a] + \frac{f''(a)}{2!}[x(n) - a]^2 + \ldots,$$

with $a = x(N)$. The 4-μm long section on which the fitting was done usually contained from 40 to 60 array members. The Taylor series was cut off after the third term. The coefficients $f(a)$, $f'(a)$, and $f''(a)$ were determined by least-squares fitting. The curvature ρ of the flagellum at $x(N)$, $y(N)$ is obtained as

$$\rho = \frac{f''(a)}{[1 + f'(a)^2]^{3/2}}.$$

This procedure represents an osculating fit at $a = x(N)$, by which the best values for the derivatives at $a = x(N)$ are obtained (Sommerfeld, 1947). The true local curvature at $x(N)$, $y(N)$ is thus found, not the average curvature of a more or less extended segment of the flagellum.

(*g*) The coordinates $x(N)$ and $y(N)$ were transformed into the absolute flagellar coordinates $X(N)$ and $Y(N)$.

(*h*) The values of $X(N)$, $Y(N)$, and $\rho(N)$ were stored on the diskette of the microcomputer.

The above procedure was programmed in FORTRAN 80. On the Altos microcomputer (having a clock cycle of 5 MHz) the program took ~2 min to run.

Our thanks are due to Dr. Richard Kleinhenz and Mrs. Isabel Nirenberg for constructing the interfacing of the various digital components and for advice with the general design of the apparatus.

This investigation was supported in part by the National Science Foundation through grant PCM-80-3700.

Received for publication 23 March 1984 and in final form 27 September 1984.

REFERENCES

Brokaw, C. J. 1972. Computer simulation of flagellar movement. I. Demonstration of stable bend propagation and bend initiation by the sliding filament model. *Biophys. J.* 12:564–586.

Brokaw, C. J. 1966. Effects of increased viscosity on the movements of some invertebrate spermatozoa. *J. Exp. Biol.* 45:113–139.

Brokaw, C. J., and R. Josslin. 1973. Maintenance of constant wave parameters by sperm flagella at reduced beat frequencies. *J. Exp. Biol.* 59:617–628.

Brokaw, C. J., and D. R. Rintala. 1974. Computer simulation of flagellar movement. III. Models incorporating cross-bridge kinetics. *J. Mechanochem. Cell Motil.* 3:77–86.

Coakley, C. J., and M. E. J. Holwill. 1973. Effects of pressure and temperature changes on the flagellar movement of *Crithidia Oncopelti*. *J. Exp. Biol.* 60:605–629.

Cosson, M. P., W. J. Y-Tang, and I. R. Gibbons. 1983. Modification of flagellar waveform and adenosine triphosphatase activity in reactivated sea urchin sperm treated with *N*-ethylmaleimide. *J. Cell Sci.* 60:231–249.

Eykhout, P., and R. Rikmenspoel. 1960. High speed flash cinemicrography applied to studies on the movement of bull spermatozoa. *Res. Film.* 3:304–312.

Gibbons, B. H., and I. R. Gibbons. 1984. Lithium reversibly inhibits microtubule-based motility in sperm flagella. *Nature (Lond.).* 309:560–562.

Gibbons, I. R. 1981. Cilia and flagella of eukaryotes. *J. Cell Biol.* 91(3, Pt. 2):107s–124s.

Gibbons, I. R., and B. H. Gibbons. 1980. Transient flagellar waveforms during intermittent swimming in sea urchin sperm. I. Wave parameters. *J. Muscle Res. Cell Motil.* 1:31–59.

Goldstein, S. F. 1979. Starting transients in sea urchin sperm flagella. *J. Cell Biol.* 80:61–68.

Goldstein, S. F. 1975. Morphology of developing bends in sperm flagella. *In* Swimming and Flying in Nature. T. Y.-T Wu, C. J. Brokaw, and C. Brennen, editors. Plenum Publishing Co., New York. 1:127–132.

Gray, J. 1955. The movement of sea urchin spermatozoa. *J. Exp. Biol.* 32:775–801.

Higgins, J., R. Frenkel, E. Hulme, A. Lucas, and G. Rangoras. 1973. The control theoretical approach to the analysis of glycolytic oscillations. *In* Biological and Biochemical Oscillators. B. Chance, A. K. Ghosh, E. K. Pye, and B. Hess, editors. Academic Press, Inc., New York and London. 127–175.

Hines, M., and J. J. Blum. 1978. Bend propagation in flagella. I. Derivation of equations of motion and their simulation. *Biophys. J.* 23:41–57.

Hines, M., and J. J. Blum. 1979. Bend propagation in flagella. II. Incorporation of dynein cross bridge kinetics into the equations of motion. *Biophys. J.* 25:421–441.

Hiramoto, Y., and S. A. Baba. 1978 A quantitative analysis of flagellar movement in enchinoderm spermatozoa. *J. Exp. Biol.* 76:85–104.

Huxley, A. F. 1957. Muscle structure and theories of contraction. *Prog. Biophys. Mol. Biol.* 7:255–318.

Johnson, D., N. R. Silvester, and M. E. J. Holwill. 1979. An analysis of the shape and propagation of waves on the flagellum of *Crithidia oncopelti. J. Exp. Biol.* 80:299–315.

Lubliner, J., and J. J. Blum. 1972. Model for bend propagation in flagella. *J. Theor. Biol.* 31:1–19.

Machin, K. E. 1958. Wave propagation in flagella. *J. Exp. Biol.* 35:796–806.

Pringle, J. W. S. 1967. The contractile mechanism of insect fibrillar muscle. *Progress Biophys.* 17:1–60.

Okuno, M., and C. J. Brokaw. 1981. Effects of Triton-extraction conditions on beat symmetry of sea urchin sperm flagella. *Cell Motil.* 1:363–370.

Okuno, M., and C. J. Brokaw. 1979. Inhibition of movement of Triton-demembranated sea urchin sperm flagella by Mg^{2+}, ATP^{4-}, ADP and P_i. *J. Cell Sci.* 38:105–123.

Rikmenspoel, R. 1985. Movements and active moments of bull sperm flagella as a function of temperature and viscosity. *J. Exp. Biol.* In press.

Rikmenspoel, R. 1982. Ciliary contractile model applied to sperm flagellar motion. *J. Theor. Biol.* 96:617–645.

Rikmenspoel, R. 1978*a*. Movement of sea urchin sperm flagella. *J. Cell Biol.* 76:310–322.

Rikmenspoel, R. 1978*b*. The equation of motion for sperm flagella. *Biophys. J.* 23:177–206.

Rikmenspoel, R. 1976. Contractile events in the cilia of *Paramecium, Opalina, Mytilis* and *Phragmatopoma. Biophys. J.* 16:445–470.

Rikmenspoel, R. 1971. Contractile mechanisms in flagella. *Biophys. J.* 11:446–463.

Rikmenspoel, R. 1966. Elastic properties of the sea urchin sperm flagellum. *Biophys. J.* 6:471–479.

Rikmenspoel, R., and W. G. Rudd. 1973. The contractile mechanism in cilia. *Biophys. J.* 13:955–993.

Sommerfeld, A. 1947. Volesungen über theoretische Physik. Vol. VI. Dieterich'sche Verlagsbuchhandel, Wiesbaden, Federal Republic of Germany.

Summers, K., and I. R. Gibbons. 1971. Adenosine triphosphate induced sliding of tubules in trypsin treated flagella of sea urchin sperm. *Proc. Natl. Acad. Sci. USA* 68:3092–3096.

Wiener, N. 1963. Time series. MIT Press, Cambridge, MA.

Yano, Y., and T. Miki-Nourmura. 1980. Sliding velocity between outer doublet microtubules of sea urchin sperm axonemes. *J. Cell Sci.* 44:169–186.